Advanced Ceramics Progress: Vol. 10, No. 3, (Summer 2024) 45-51

Materials and Energy Research Center
MERC

Contents lists available at ACERP

Advanced Ceramics Progress

Journal Homepage: www.acerp.ir

Original Research Article

Structural and Magnetic Characterization of Cobalt Ferrite Nanofibers Produced by Electrospinning Method

Zahra Rahmani Boldaji [a]*, Ali Ghasemi [b], Shahab Torkian [c], Mahdieh Akbari Gandomani [a]

[a] *Master, Department of Materials Engineering, Malek Ashtar University of Technology, Shahin Shahr, Isfahan, Iran.*
[b] *Professor, Department of Materials Engineering, Malek Ashtar University of Technology, Shahin Shahr, Isfahan, Iran.*
[c] *Assistant Professor, Department of Materials Engineering, Malek Ashtar University of Technology, Shahin Shahr, Isfahan, Iran.*

* Corresponding Author Email: zah.ra.hmani111@gmail.com (Zahra. Rahmani Boldaji) URL: https://www.acerp.ir/article_212950.html

ARTICLE INFO

Article History:
Received: 01 November 2024
Revised: 23 November 2024
Accepted: 07 January 2025

Keywords:
$CoFe_2O_4$,
Electrospun Fibers,
Magnetic Ceramics,
Nanomaterials

ABSTRACT

Cobalt ferrite, with the general formula $CoFe_2O_4$, exhibits unique magnetic properties such as high magnetocrystalline anisotropy, high coercive field, intermediate saturation magnetization, and excellent physical and chemical stability. Moreover, the use of nanofibers in the field of magnetic materials is increasingly popular due to their high surface-to-volume ratio, low weight, high porosity, and considerable shape anisotropy. In this research, cobalt ferrite nanofibers with different diameters were produced via electrospinning using a solution containing 8 wt% polyvinylpyrrolidone, with the applied voltage being optimized. Based on the results of energy dispersive spectroscopy (EDS), the presence of Fe, O, and Co elements in the structure of the cobalt ferrite nanofibers was confirmed. Additionally, X-ray diffraction (XRD) analysis revealed that the cobalt ferrite nanofibers are formed in a single phase after calcination at 800 °C. Field emission scanning electron microscopy (FE-SEM) images showed that, by optimizing the applied voltage between the nozzle and the collector, the average diameters of the cobalt ferrite nanofibers were varied between 86 nm and 171 nm. According to vibrating sample magnetometry (VSM), the saturation magnetization, residual magnetization, and coercive field of the optimized sample were measured as 85 A·m²/kg, 61 A·m²/kg, and 1.32×10^5 A/m, respectively. First-order reversal curve (FORC) results showed that increasing the average diameter of the fibers raises magnetostatic interaction. Based on the results of this research, the production of cobalt ferrite nanofibers using the electrospinning method is feasible. Compared to similar studies, higher values of saturation magnetization and coercive field were obtained in this work.

https://doi.org/10.30501/acp.2025.486481.1167

1. INTRODUCTION

Magnetic ceramics have gained considerable attention in various scientific and technological fields, including hyperthermia, magnetic recording, dye removal, magnetic resonance imaging (MRI), and catalysis in organic synthesis (Chermahini et al., 2019). Among these, ferrites stand out for their unique structural properties, offering significant potential in applications such as magnetic hyperthermia and catalysis (Conceição et al., 2024). Ferrite nanoparticles, with their high specific absorption rates, are particularly suitable for hyperthermia and other heat-related applications (Dala et al., 2024). Moreover, ferrites hold promise in areas such as MRI and electronic devices (Khalil et al., 2024). Additionally, magnetic nanocomposites, which demonstrate enhanced thermal conductivity under magnetic fields, are being explored for use in hyperthermia and thermal management (Alsangur et al., 2024). These materials also serve as actuators, sensors, and transformer components due to their low eddy

Please cite this article as: Rahmani Boldaji, Z., Ghasemi, A., Torkian, Sh. & Akbari Gandomani, M. (2024). Structural and Magnetic Characterization of Cobalt Ferrite Nanofibers Produced by Electrospinning Method, *Advanced Ceramics Progress*, 10(3), 45-51. https://doi.org/10.30501/acp.2025.486481.1167

current dissipation and excellent performance in the radio frequency band (Das et al., 2023). Researchers are keen to explore these ceramics in different forms, such as bulk, films, or nanopowders, produced through various processes, doped with different cations, and annealed at diverse temperatures. Nanostructures are being fabricated using distinct synthesis methods like electrospinning, sol-gel, chemical methods, hydrothermal methods, and electrodeposition techniques (Peng et al., 2023; Martinson et al., 2022). Among these, electrospun nanofibers from magnetic materials form a magnetic network, which is useful for neuromorphic computing and other novel applications (Amini et al., 2021). Polymer matrix-based nanofibers synthesized by electrospinning represent a significant area of current research and development. One-dimensional magnetic nanofibers are especially attractive due to their unique structural characteristics and the combination of magnetic and electrical properties with chemical and thermal stability. Numerous methodologies for nanofiber production are available, including vapor deposition polymerization (VDP), chemical vapor deposition (CVD), and supercritical fluid techniques. However, these methods are often not economically feasible, yield irregular nanofibers, and involve more complex synthesis processes compared to electrospinning (Anwar et al., 2023). Electrospinning stands out as a straightforward and cost-effective technique that allows for precise control over nanostructure dimensions and properties by adjusting parameters such as electric field, solution viscosity, humidity, and sintering temperature (Miao et al., 2010). Among the various synthesis techniques, electrospinning offers a facile and versatile method for fabricating $CoFe_2O_4$ into nanoscale fibrous morphologies (Guan et al., 2021). This technique provides numerous advantages, including the ability to control the size of the nanostructures, high aspect ratios, and cost efficiency (Ju et al., 2008). Electrospinning can produce ferrite fibers with diameters ranging from nanometers to several micrometers, arranged in random or organized fashions (Wang et al., 2008). Conversely, ferrites, with the general formula AFe_2O_4 (where A = Ni, Mn, Co, Cu, or Zn), are significant magnetic materials due to their magnetic and electrical properties, chemical, and thermal toughness (Anwar et al., 2023). These materials are employed in applications such as high-density recording systems, microwave absorbers, targeted drug delivery systems, and magnetic sensors. One-dimensional ferrite nanostructures, in particular, are important for their unique magnetic properties due to their long axial ratios (Ju et al., 2008). The manufacturing methods, particle size, shape, annealing temperature, and cation distribution significantly impact the magnetic characteristics of spinel ferrite nanofibers (Anwar et al., 2023). Among various ferrites, cobalt ferrite ($CoFe_2O_4$) has been extensively investigated due to its significant magnetocrystalline anisotropy, high coercivity, notable magnetostriction, chemical stability, and unique combination of magnetic and dielectric properties (Mansour et al., 2020). CFO can be fabricated into various morphologies, designed to prevent aggregation and obtain high surface areas and porosities (Guan et al., 2021). Ju et al. (2008) and Wang et al. (2008) developed and characterized $CoFe_2O_4$ nanofibers, investigating their structural and magnetic properties under varying calcination temperatures (Ju et al., 2008; Wang et al., 2008). Sangmanee et al. (2009) and Pan et al. (2011) further studied the effects of calcination temperature and heating rate on these nanofibers' morphology and magnetic properties (Sangmanee et al., 2009; Pan et al., 2011). Liu et al. (2015) highlighted their superior catalytic efficiency for hydrazine detection (Liu et al., 2015), while Prasad et al. (2019) demonstrated their gas sensing capabilities for various gases at room temperature (Durga Parasad et al., 2019). Liu et al. (2020) examined how annealing temperature affects cation distribution, influencing diameter and morphology (Liu et al., 2020). This research aims to synthesize $CoFe_2O_4$ fibers through the electrospinning technique using a DMF/ethanol precursor solution containing PVP and metal nitrates, while also analyzing their structural, morphological, and enhanced magnetic properties. The effects of voltage on nanofiber diameter and its influence on magnetic properties are investigated, along with a detailed discussion of the structural, morphological, and magnetic properties of the synthesized fibers.

2. MATERIALS AND METHODS

1.2. Materials

Cobalt (II) nitrate hexahydrate (99%, Merck Co.) and iron (III) nitrate nonahydrate (99%, Merck Co.) were used as metal precursors. Citric acid anhydrous ($C_6H_8O_7 \cdot H_2O$, 99%, Merck Co.) was employed as a chelating agent. Polyvinylpyrrolidone (PVP, M_w = 500,000, Merck Co.) was used as a polymer-based matrix. N, N-dimethylformamide (DMF, 99.5%, Merck Co.), ethanol (C_2H_5OH, 99.5%, Merck Co.), and deionized water were used as solvents.

2.2. Synthesis

The formation of cobalt ferrite nanofibers is a three-step process. Initially, the cobalt ferrite precursor solution is prepared using the sol-gel method. This solution is then filled into a plastic syringe equipped with a metal needle, which is subsequently placed in an electrospinning device. After electrospinning, the obtained fibers undergo heat treatment. To produce a precursor solution with 8 wt% PVP, a specific amount of PVP was added to a mixture of ethanol and deionized water. Once the PVP was completely dissolved using a magnetic stirrer, another solution containing 1.7 g of cobalt nitrate hexahydrate, 4.8 g of iron nitrate nonahydrate, 2.8 g of citric acid monohydrate, 10 ml of dimethylformamide, and 5 ml of deionized water was gently added to it while stirring. The mixture was stirred

for 20 hours at room temperature to achieve a solution with optimum viscosity. The syringe filled with the solution was then loaded into the electrospinning device. The distance between the aluminum collector and the needle tip was set at 19 cm, with a solution flow rate of 0.3 ml/h under an applied voltage of 13, 15, and 17 kV, and the obtained samples were named A, B, and C, respectively. The as-spun fibers were dried at 200 °C for 5 hours and then calcined at 800 °C for 3 hours in air.

3.2. Characterization

The nanofibers produced were subjected to X-ray diffraction (XRD) analysis using an X'Pert Pro X-ray diffractometer (ASENWARE). The analysis was conducted with Cu Kα radiation (λ = 0.154 nm) at a generator voltage of 40 kV. The morphology of the electrospun nanofibers was investigated using field emission scanning electron microscopy (FE-SEM: MIRA3 TE-SCAN). Additionally, energy-dispersive X-ray spectroscopy (EDS) analysis was performed to semi-quantitatively determine the chemical composition of the strontium nanofibers. The hysteresis loops were measured at ambient temperature by applying a vibrating sample magnetometer (VSM; Meghnatis Daghigh Kavir Co., Iran). FORC diagrams were also performed to thoroughly interpret coercivity, magneto-static interaction field distributions, and magnetic phases.

3. RESULTS AND DISCUSSION

3.1. Structural Investigation

Figure 1(a) illustrates the X-ray diffraction pattern of cobalt ferrite nanofibers. As indicated in the figure, the nanofibers's crystal structure was shaped by the calcination process at 800°C for 3 hours. Notably, all primary peaks, namely (220), (311), and (400), have been successfully indexed to $CoFe_2O_4$ without presenting any undesirable phases. Moreover, all diffraction peaks are narrow and sharp, indicating high crystallinity. This phase is associated with the face-centered cubic spinel configuration, as evidenced by the standard data (00-022-1086). There is an absence of any secondary or impurity peaks across samples, corroborating their phase purity. Additionally, the lattice parameters and crystallite sizes have been derived using Equations (1) and (2) [13], with the results detailed in Table 1.

TABLE 1. The lattice parameter, average size of crystallites calculated from XRD results

Sample	Lattice parameter (nm)	Average crystallite size (nm)	Crystallinity
A	0.98	51.57	24.5
C	0.99	63.47	16.5

TABLE 2. Average fiber diameter electrospun at three different applied voltages

Sample	Applied voltage (kV)	Average fiber diameter (nm)
A	13	86
B	15	140
C	17	171

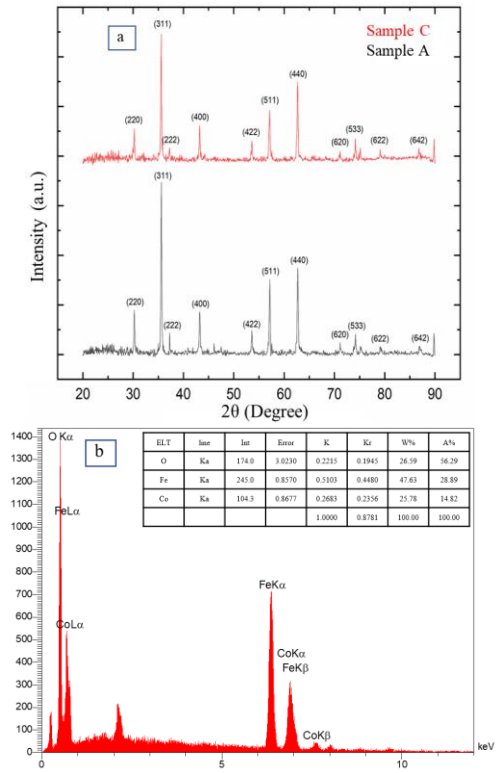

Figure 1. (a) X-ray diffraction pattern of $CoFe_2O_4$ nanofiber samples A and C (Table 2). (b) Diagram of the energy dispersive spectroscopy (EDS) for cobalt ferrite nanofibers and the obtained elemental analysis

$$\sin^2(\theta) = \left(\frac{\lambda^2}{4a^2}\right)\left(h^2 + k^2 + l^2\right) \quad (1)$$

$$\beta = \frac{k\lambda}{L\cos\theta} \quad (2)$$

In Equation (1), θ is the Bragg angle, λ is the wavelength of the X-ray used, a is the lattice parameter, and h, k, l are the Miller indices, indicating the crystal plane orientations. In Equation (2), β represents the full width at half maximum (FWHM) of the diffraction peak, λ signifies the X-ray wavelength in nanometers (nm), L denotes the crystallite size, and K is a constant related to the crystallite shape, conventionally assumed to be 0.89.

To analyze the elemental composition of $CoFe_2O_4$ nanofibers, EDS analysis was conducted. The results are displayed in Figure 1(b).

3.2. Morphological Study

Figure 2 shows FE-SEM images of the electrospun $CoFe_2O_4$ fibers. Morphological studies confirmed the formation of a continuous, bead-free fiber structure in the calcined samples. After calcination at 800°C, a structure of packed particles or crystallites became prominent. As shown in Table 3, the diameter of the calcined fibers increased from 86 nm up to 171 nm with an increase in the applied voltage from 13 kV to 17 kV. The surface of the $CoFe_2O_4$ fibers is uneven and rough, which is

attributed to the removal of PVP and the nucleation of $CoFe_2O_4$ (Durga Parasad et al., 2019). A longer flight time allows more time for the fibers to stretch and elongate before being deposited on the collector. Thus, at a lower voltage, the reduced acceleration of the jet and weaker electric field may increase the flight time of the electrospinning jet, which may favor the formation of finer fibers (Ramakrishna et al., 2005). Additionally, by increasing the applied voltage (i.e., increasing the electric field strength), more solution is removed from the capillary tip as the jet is ejected from the Taylor cone. This results in an increase in fiber diameter (Haghi, 2012).

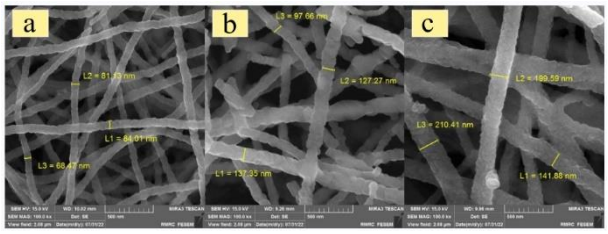

Figure 2. FE-SEM images of nanofibers electrospun at different applied voltages (a) 13 kV, (b) 15 kV and (c) 17 kV

TABLE 3. Comparison of Magnetic Properties of Cobalt Ferrite Nanofibers Produced at Various Electrospinning Voltages and Results from Other Studies

Sample	M_S (A.m^2/kg) & (emu/g)	M_r (A.m^2/kg) & (emu/g)	H_c (A/m) (Oe)	M_r / M_s
A	85	41	1.32 × 10^5 1659	0.48
B	62	31	1.19 × 10^5 1500	0.5
C	58	29	1.12 × 10^5 1407	0.5
(Ju et al., 2008)	78.6	32.5	6.26 × 10^4 786.5	0.41
(Khalil et al., 2024)	76.2	38.86	7.56 × 10^4 950	0.51
(Sangmanee et al., 2009)	71.7	35.9	6.85 × 10^4 860.6	0.5
(Durga Parasad et al., 2019)	76.5	32.13	7.83 × 10^4 984	0.42
(Liu et al., 2020)	82.1	-	8.54 × 10^4 1073	-

3.3. Magnetic Properties

The magnetic behavior of a nanoparticle assembly varies with the morphology of the particles (particle size and shape) and is strongly influenced by interparticle interactions. The magnetic interactions can result from dipolar coupling and exchange coupling among the nanoparticles' surface atoms and play a fundamental role in the physics of these systems (Wang et al., 2008). Figure 3 shows the magnetic hysteresis loops of the samples electrospun at three different applied voltages. All three exhibited the typical hysteresis loops of hard magnetic behavior, demonstrating that the presence of an ordered magnetic structure exists in the spinel system, as explained by Liu et al. (Liu et al., 2005). Magnetic data are summarized in Table 4. The saturation magnetization, remanence magnetization, and coercivity of the sample electrospun at 13 kV with an average diameter of 86 nm were 85 A· m^2/kg, 41 A·.m^2/kg, and 1.32×10^5 A/m, respectively. Compared with our previous work, where $Co_2Fe_2O_4$ was prepared by the sol-gel auto-combustion method (Torkian et al., 2017), in which the values were 89 A.m^2/kg, 20 A.m^2/kg, and 5.17×10^5 A/m, respectively, the coercivity has clearly increased due to the effect of shape anisotropy in the nanofibers, as indicated by Equation (3). Furthermore, the M_s, M_r, and H_c of the samples electrospun at 15 kV and 17 kV with average diameters of 140 nm and 171 nm were 62 A.m^2/kg, 31 A.m^2/kg, and 1.19×10^5 A/m, and 58 A.m^2/kg, 29 A.m^2/kg, and 1.12×10^5 A/m, respectively.

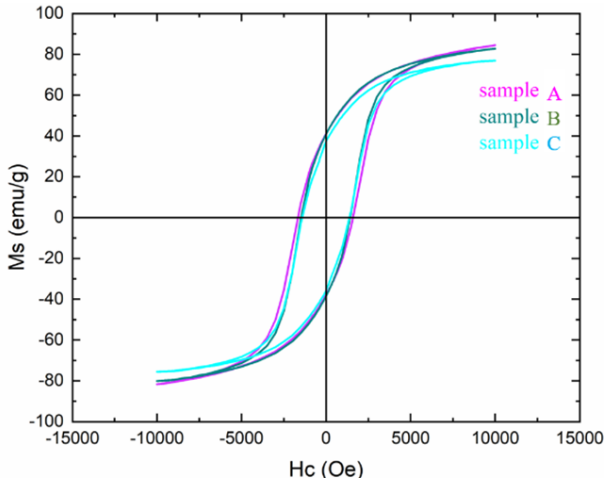

Figure 3. Hysteresis loops of samples with applying different voltages during electrospinning

TABLE 4. Magnetic properties of samples with applying different voltages during electrospinning

Sample	Average fiber diameter (nm)	FWHM (A/m) (Oe)	H_c (A/m) (Oe)	$H_{C,max}^{FORC}$ (A/m) (Oe)
A	85	5.46×10^5	1.32×10^5	1.58×10^5
		686	1650	1994
B	62	6.13×10^5	1.19×10^5	1.35×10^5
		772	1500	1703
C	58	6.68×10^5	1.12×10^5	1.38×10^5
		840	1407	1747

These variations are due to changes in the nanofibers' diameters:

$$H_c \approx \frac{2K_{eff}}{M_s} \quad (3)$$

where K_{eff} is the effective anisotropy constant, which includes contributions from shape anisotropy, and M_s the saturation magnetization of the material. Coercivity decreases as the applied voltage increases. Sample A, with the smallest diameter (86 nm), exhibits the highest coercivity (1.32×10^5 A/m), while Sample C, with the largest diameter (171 nm), shows the lowest coercivity (1.12×10^5 A/m). The relationship between coercivity (H_c) and the diameter of magnetic fibers is explained by the theory of magnetization reversal by curling. According to this theory, coercivity increases with a decrease in the fiber diameter squared, or $H_c \propto 1/d^2$. This relationship arises because thinner fibers have a higher surface-to-volume ratio, which enhances the influence of surface and interface effects on the magnetic behavior of the material (Stöckel et al., 1980). Saturation magnetization (M_s) and remanent magnetization (M_r) also show a decreasing trend with increasing fiber diameter. Sample A has the highest M_s (85 A.m^2/kg) and M_r (41 A.m^2/kg), while Sample C has the lowest M_s (58 A.m^2/kg) and M_r (29 A.m^2/kg). The reduction in M_s with increasing fiber diameter can be attributed to the decreased interaction between magnetic domains in thicker fibers (Stöckel et al., 1980).

The relationship between fiber diameter, crystallinity, and M_s in nanofibers is well-documented. As shown in Table 1, nanofibers with smaller diameters tend to have higher crystallinity and, consequently, higher M_s. This is due to the increased surface-area-to-volume ratio in smaller fibers, which promotes better crystallinity and alignment of magnetic domains (Taufiq et al., 2019; Li et al., 2014).

The ratio M_r/M_s remains fairly constant at around 0.5, indicating that the remanence relative to the saturation remains similar despite changes in diameter. The magnetic properties of our samples were compared with those reported in other studies (Table 3). For instance, Ju et al. (Asplund et al., 2016) reported an M_s of 78.6 A.m^2/kg and an H_c of 6.26×10^4 A/m for cobalt ferrite nanofibers. Similarly, Ghaddar et al. (Ghaddar et al., 2010) found M_s and H_c values of 76.2 A.m^2/kg and 7.56×10^4 A/m, respectively. These values are lower than those observed in our samples, indicating that the electrospinning voltage and resulting fiber diameter significantly influence the magnetic properties.

The higher coercivity in our samples can be attributed to shape anisotropy and smaller fiber diameters, which enhance the magnetic interactions and surface effects. Figure 4 shows FORC diagrams of the samples. By studying the information obtained along the coercivity axis, the distribution of coercivity and the state of magnetic domains within the material can be determined.

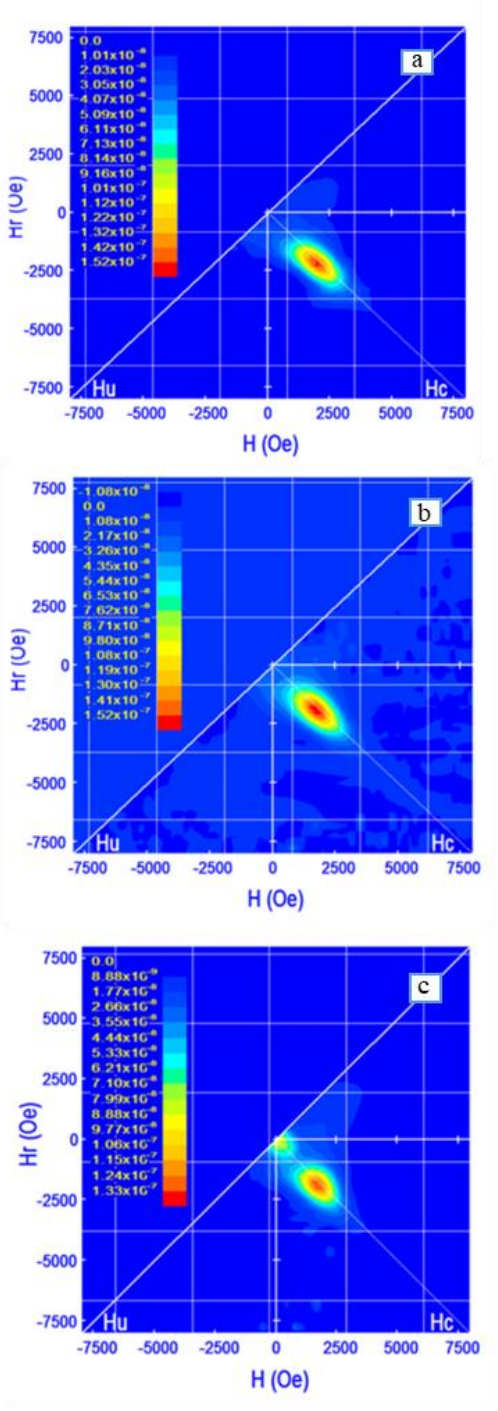

Figure 4. FORCs diagrams with applying different voltages during electrospinning (a) 13 kV, (b) 15 kV and (c) 17 kV

The more elongated the system is along this axis, the more distributed the coercivity of the particles is, indicating the presence of particles with different coercivities in the system (Asplund et al., 2016). According to the distribution diagrams shown in Figure 5 along the H_c axis for Samples A and B, it can be inferred that the structure of the nanofibers produced in these samples is single-phase.

In Table 4, the $H_{C,max}^{FORC}$ values are compared with the H_c values obtained from the hysteresis loop. According to the data in the table, the $H_{C,max}^{FORC}$ values for all three samples are higher than the H_c values obtained from the hysteresis loop. This difference arises because H_c from the hysteresis loop reflects the average coercivity of all the magnetic domains in the material, whereas FORC diagrams display a distribution of the coercivity of these domains. Specifically, $H_{C,max}^{FORC}$ represents the coercivity corresponding to the most prevalent amount among the magnetic domains (Asplund et al., 2016). Figure 5(a) illustrates the coercivity field distribution diagram for samples A, B, and C.

Elongation along the interaction axis reflects the extent of interaction between particles: the less the elongation, the weaker the particle interactions, and vice versa. The absence of elongation parallel to the H_u axis and the narrow distribution of the diagram in this direction indicate a low degree of magnetostatic interaction in the produced nanofibers (Ghaddar et al., 2010). In Table 4, a comparison of the full width at half maximum (FWHM) values for samples A, B, and C reveals that, with an increase in the average diameter of the nanofibers, the interaction distribution also increases. Figure 5(b) displays the interaction distribution diagram for all three samples.

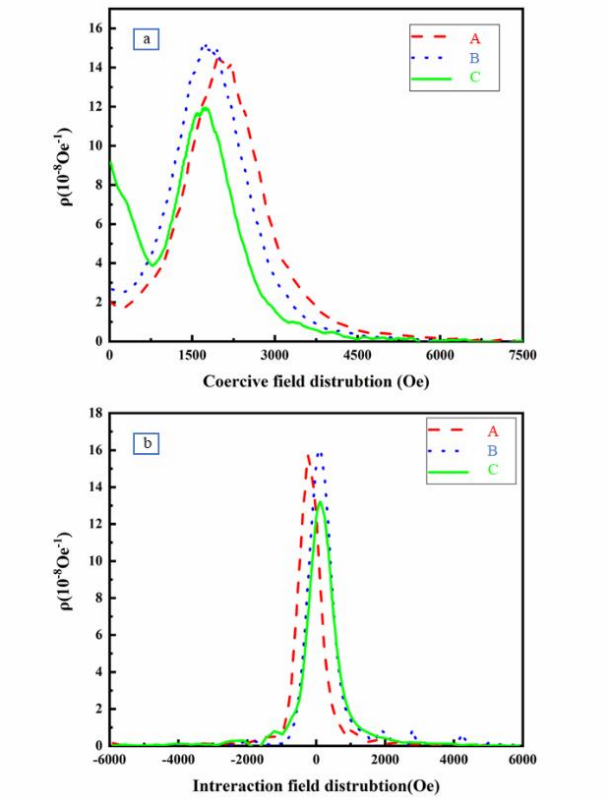

Figure 5. (a)Comparison diagram of the coercivity field distribution of nanofibers. (b) Comparison diagram of the interaction distribution of nanofibers

4. CONCLUSION(S)

This study successfully demonstrated the fabrication of cobalt ferrite nanofibers using the electrospinning method and provided a detailed analysis of their magnetic and structural properties. The optimal sample, designated as Sample A, was produced at 13 kV and exhibited an average diameter of 86 nm. This resulted in the highest observed coercivity (1.32×10^5 A/m) and saturation magnetization (85 A.m²/kg). These magnetic properties underscore the strong correlation between fiber size and coercivity, with smaller diameters contributing to increased coercivity due to the enhanced influence of shape anisotropy. In contrast, increasing the voltage to 17 kV led to larger nanofiber diameters (up to 171 nm), which were associated with stronger magnetostatic interactions, as evidenced by broader FWHM values in FORC distribution diagrams. These findings provide direct evidence that the electrospinning voltage significantly influences both the morphology and magnetic behavior of the nanofibers, enabling the fine-tuning of magnetic properties for specific applications. Therefore, this study emphasizes the importance of controlling electrospinning parameters to engineer cobalt ferrite nanofibers with desirable properties for various magnetic applications.

ACKNOWLEDGEMENTS

We gratefully acknowledge Department of Materials Engineering, Malek Ashtar University of Technology, Isfahan, Iran for financial support.

NOMENCLATURE

a	Lattice parameter
CFO	Cobalt ferrite
$CoFe_2O_4$	Cobalt ferrite
CVD	Chemical vapor deposition
d	Diameter of magnetic fibers
DMF	N, N-dimethylformamide, a solvent
EDS	Energy-dispersive X-ray spectroscopy
FE-SEM	Field emission scanning electron microscopy
FORC	First-order reversal curve
FWHM	Full width at half maximum of a peak
H_c	Coercivity
$H_{C,max}^{FORC}$	Coercivity associated with the most prevalent coercivity amount of magnetic domains
H_u	The interaction field in First-order Reversal Curve analysis
K	A constant linked to crystallite shape
K_{eff}	Effective anisotropy constant
L	Crystallite size
M_r	Remanence magnetization
M_s	Saturation magnetization
PVP	Polyvinylpyrrolidone, a polymer-based matrix
VDP	Vapor deposition polymerization
VSM	Vibrating sample magnetometer
XRD	X-ray diffraction
β	Full width at half maximum (FWHM) of the diffraction peak
h, k, l	Miller indices, a set of three integers that designate a specific plane or family of planes within a crystal lattice
θ	Bragg angle, the angle of incidence at which X-rays are diffracted by a crystal lattice
λ	Wavelength of the X-ray used

REFERENCES

1. Alsangur, R., Doganay, S., Ates, İ., Turgut, A., Cetin, L., & Rebay, M. (2024). Magnetic field dependent thermal conductivity investigation of water-based Fe_3O_4/CNT and Fe_3O_4/graphene magnetic hybrid nanofluids using a Helmholtz coil system setup. Diamond and Related Materials, 141, 110716. https://doi.org/10.1016/j.diamond.2023.110716
2. Amini, F., Blachowicz, T., & Ehrmann, A. (2021). Systematic study of magnetization reversal in beaded fibers from different magnetic materials. Journal of Magnetism and Magnetic Materials, 529,167862. https://doi.org/10.1016/j.jmmm.2021.167855
3. Anwar, U., Faizan, J., Rehman, U. U., Gul, M., Yasmeen, G., & Nadeem, M. (2023). Effect of sintering temperature on impedance and EMI shielding of carbon modified $CoFe_2O_4$ nanofibers via electrospinning. Ceramics International, 49(23), 38847-38854. https://doi.org/10.1016/j.ceramint.2023.09.221
4. Asplund, T., & Luengo Hendriks, C. L. (2016). A faster, unbiased path opening by upper skeletonization and weighted adjacency graphs. IEEE Transactions on Image Processing, 25(12), 5589-5600. https://doi.org/10.1109/TIP.2016.2609805
5. Chermahini, M. D., Baghbaderani, H. A., Shahraki, M. M., & Kazazi, M. (2019). Low temperature sintering of magnetic $Ni_{0.5}Co_{0.5}Fe_2O_4$ ceramics prepared from mechanochemically synthesized nanopowders. Ceramics International, 45(5), 5491-5495. https://doi.org/10.1016/j.ceramint.2018.12.005
6. Conceição, D. C. de O., Neves, R. C. S., França, E. L. T., Rodrigues, A. R., Alves Junior, S., & Padrón-Hernández, E. (2024). Development of a new method for the preparation of mesoporous magnetic nanoparticles of cobalt ferrite ($CoFe_2O_4$) with applied parameters for magnetic hyperthermia. Nano-Structures & Nano-Objects, 37, 101073. https://doi.org/10.1016/j.nanoso.2023.101073
7. Dalal, M., Greneche, J.-M., Ningthoujam, R. S., & Chakrabarti, P. K. (2024). Study of magnetic induction heating of $Li_{0.25}Zn_{0.3}Co_{0.15}Fe_{2.3}O$ nanoparticles. Materials Chemistry and Physics, 313, 128765. https://doi.org/10.1016/j.matchemphys.2023.128765
8. Das, T., Noor, S., Kumari, S., Mallick, J., Shukla, A., Datta, S., Manglam, M. K., & Kar, M. (2023). Tuning of magnetic properties of Al-doped cobalt ferrite nanofiber prepared by electrospinning technique. Physica Scripta, 98(8). https://doi.org/10.1088/1402-4896/ace802
9. Durga Prasad, P., & Hemalatha, J. (2019). Enhanced magnetic properties of highly crystalline cobalt ferrite fibers and their application as gas sensors. Journal of Magnetism and Magnetic Materials, 484, 225-233. https://doi.org/10.1016/j.jmmm.2019.04.026
10. Ghaddar, A., Gloaguen, F., & Gieraltowski, J. (2010). Magnetic properties of ferromagnetic nanowire arrays: Theory and experiment. Journal of Physics: Conference Series, 200(7), 072032. https://doi.org/10.1088/1742-6596/200/7/072032
11. Guan, Z.-Y., Kwon, E., Lee, J., Lin, Y.-F., & Lin, K.-Y. A. (2021). Electrospun cobalt ferrite nanofiber as a magnetic and effective heterogeneous catalyst for activating peroxymonosulfate to degrade sulfosalicylic acid. Separation and Purification Technology, 259, 117037. https://doi.org/10.1016/j.seppur.2020.118163
12. Haghi, A. K. (2012). Electrospinning of nanofibers in textiles. Apple Academic Press, Inc. https://doi.org/10.1201/b12229
13. Ju, Y.-W., Park, J.-H., Jung, H.-R., Cho, S.-J., & Lee, W.-J. (2008). Fabrication and characterization of cobalt ferrite ($CoFe_2O_4$) nanofibers by electrospinning. Materials Science and Engineering: B, 147(1), 7-12. https://doi.org/10.1016/j.mseb.2007.10.018
14. Khalil, H. F., Gad, S., Fakhry, F., & Elsharkawy, S. G. (2024). Role of Cr^{3+} and In^{3+} ions substitution on magnetic and dielectric properties for developing soft magnetic M-Type Sr nanohexaferrite. Materials Science in Semiconductor Processing, 169, 107896. https://doi.org/10.1016/j.mssp.2023.107896
15. Li, X. J., Wei, Q., & Wang, X. (2014). Preparation of magnetic polyimide/maghemite nanocomposite fibers by electrospinning. High Performance Polymers, 26(7), 810-816. https://doi.org/10.1177/0954008314530449
16. Liu, X. M., Fu, S. Y., Xiao, H. M., & Huang, C. J. (2005). Synthesis of nanocrystalline spinel $CoFe_2O_4$ via a polymer-pyrolysis route. Physica B: Condensed Matter, 370(1-4), 14-21. https://doi.org/10.1016/j.physb.2005.08.030
17. Liu, J., Shen, J., Li, M., & Guo, L. P. (2015). A high-efficient amperometric hydrazine sensor based on novel electrospun $CoFe_2O_4$ spinel nanofibers. Chinese Chemical Letters, 26(12), 1478–1484. https://doi.org/10.1016/j.cclet.2015.10.026
18. Liu, N., Zhang, Y., Wang, H., Yang, M., & Chen, J. (2020). Controllable synthesis of $CoFe_2O_4$ electrospun nanofibers. CrystEngComm, 22(10), 1839-1847. https://doi.org/10.1039/C9CE01825E
19. Mansour, S. F., Imam, N. G., Goda, S., & Abdo, M. A. (2020). Constructive coupling between $BiFeO_3$ and $CoFe_2O_4$; promising magnetic and dielectric properties. Journal of Materials Research and Technology, 9(2), 1434-1446. https://doi.org/10.1016/j.jmrt.2019.11.069
20. Martinson, K. D., Belyak, V. E., Sakhno, D. D., Ivanov, A. A., Lebedev, L. A., Nefedova, L. A., & Karpinsky, D. V. (2022). Solution combustion assisted synthesis of ultra-magnetically soft LiZnTiMn ferrite ceramics. Journal of Alloys and Compounds, 894, 162554. https://doi.org/10.1016/j.jallcom.2021.162554
21. Miao, J., Miyauchi, M., Simmons, T., Dordick, J., & Linhardt, R. (2010). Electrospinning of nanomaterials and applications in electronic components and devices. Journal of Nanoscience and Nanotechnology, 10, 5507-5519. https://doi.org/10.1166/jnn.2010.3073
22. Pan, W., Ma, Z., Liu, J., Liu, Q., & Wang, J. (2011). Effect of heating rate on morphology and structure of $CoFe_2O_4$ nanofibers. Materials Letters, 65(21–22), 3269–3271. https://doi.org/10.1016/j.matlet.2011.06.102
23. Peng, H., Yang, P., Yang, P., & Qi, H. (2023). Design, fabrication, and magnetic properties of novel (Ni, Cr, Zr)-co-doped M-type barium ferrite ceramics. Ceramics International, 49(13), 21577-21586. http://dx.doi.org/10.1016/j.ceramint.2023.03.294
24. Ramakrishna, K. F. S., Teo, W.-E., Lim, T.-C., & Ma, Z. (2005). An introduction to electrospinning and nanofibers. World Scientific Publishing Co. Pte. Ltd. https://doi.org/10.1142/9789812567611
25. Sangmanee, M., & Maensiri, S. (2009). Nanostructures and magnetic properties of cobalt ferrite ($CoFe_2O_4$) fabricated by electrospinning. Applied Physics A: Materials Science & Processing, 97(1), 167–177. https://doi.org/10.1007/s00339-009-5256-5
26. Stöckel, D. a. N. (1980). Magnetische Messungen an Faserverbundwerkstoffen. Materialwissenschaft und Werkstofftechnik, 11, 217-223. https://doi.org/10.1002/mawe.19800110608
27. Taufiq, A., Ainun Jannah, M., Hidayat, A., Hidayat, N., Mufti, M. N., & Susanto, H. (2019). Structural and magnetic behaviours of magnetite/polyvinyl alcohol composite nanofibers. IOP Conference Series: Materials Science and Engineering, 515, 012081. https://doi.org/10.1088/1757-899X/515/1/012081
28. Torkian, S., Ghasemi, A., & Razavi, R. (2017). Cation distribution and magnetic analysis of wideband microwave absorptive $CoxNi1-xFe_2O_4$ ferrites. Ceramics International, 43. https://doi.org/10.1016/j.ceramint.2017.02.124
29. Wang, X. L., Lv, M., Chai, P., Liu, Y., Zhou, X., & Meng, J. (2008). Preparation of one-dimensional $CoFe_2O_4$ nanostructures and their magnetic properties. The Journal of Physical Chemistry C, 112(27), 15171–15175. https://doi.org/10.1021/jp802614v